Divalent cation diffusion in calcium fluorapatite

Eleanor E. Jay · Phillip M. Mallinson ·
Shirley K. Fong · Brian L. Metcalfe ·
Robin W. Grimes

Abstract The mechanisms by which calcium ions are transported through the fluorapatite lattice are investigated using computer simulations. Cation vacancy assisted pathways are considered and migration energy barriers are calculated using a nudged elastic band transition state search. Migration activation energies for a range of divalent cations, in addition to calcium are compared. Generally there is very little change in activation energy as cation radius increases. Furthermore, in all cases the lowest energy migration pathways occur parallel to the c-axis either associated with the central anion channel via Ca(2) sites or away from the channel and via Ca(1) sites.

Introduction

Apatite minerals are of interest as potential nuclear waste hosts. This is due to both the thermal and chemical stability of the mineral over geological timescales and the ability of apatite mineral phases to adopt a wide range of compositions and stoichiometries [1]. This allows considerable compositional flexibility and offers the potential to dissolve and immobilise radioisotopes, in the presence of halides, which are difficult to accommodate in traditional vitreous or cement type waste forms [2]. Furthermore, there is great interest in the migration of cations with respect to biomaterial applications; fluorapatite is one of the constituents of teeth and bones. The control of caries production in teeth would benefit from a knowledge of cation migration [3].

The naturally occurring mineral apatite exhibits space group $R6_3/m$ [4] and its chemical formula is described as: $A_{10}(XO_4)_6B_2$ [5], where the most common anionic groups, B^-, are: F, OH or Cl while A = Ca, Sr, Pb, Na, etc. and X = P, As, Si, V, etc. [6]. The primary crystallographic description of fluorapatite was provided by Beevers and McIntyre [7], who identified these two key features. Firstly, the presence of a central tunnel structure, which is orientated along the c-axis, with CaO_6 and PO_4 polyhedra as corner connected units (see Fig. 1); secondly, that the tunnels are occupied by anions (OH^-, Cl^-, F^-). In this study we will investigate fluorapatite (FAp) so the anion member is F^- and X is the P^{5+} ion.

There are two types of Ca site in FAp. The first is a sevenfold coordinated Ca(1) (or 4f) site, which creates two triangular formations on mirror planes. The other is a ninefold coordinated Ca(2) (or 6h) site, which is linked with phosphate groups forming a hexagonal network [5] (see Fig. 1).

Beevers and McIntyre [7] concluded that even very minor changes in the atomic radii of cation species within the c-axis tunnel lead to an expansion or contraction of the tunnel. Therefore, it is useful to consider mechanisms and energies for cation migration within the lattice. Furthermore, atomic diffusion via a given mechanism is rate limited by the largest activation barrier separating two minimum energy atomic configurations. It is the rate limiting process that will impact upon the suitability of the mineral phase as a potential waste form, where leeching of elements must be minimised [8].

Here atomic scale simulations are used to calculate these migration pathways and identify the lowest energy and rate limiting step in FAp. To identify barriers we employed a

E. E. Jay · R. W. Grimes (✉)
Department of Materials, Imperial College London,
London SW7 2AZ, UK
e-mail: r.grimes@ic.ac.uk

P. M. Mallinson · S. K. Fong · B. L. Metcalfe
Materials Science Research Division, AWE, Aldermaston,
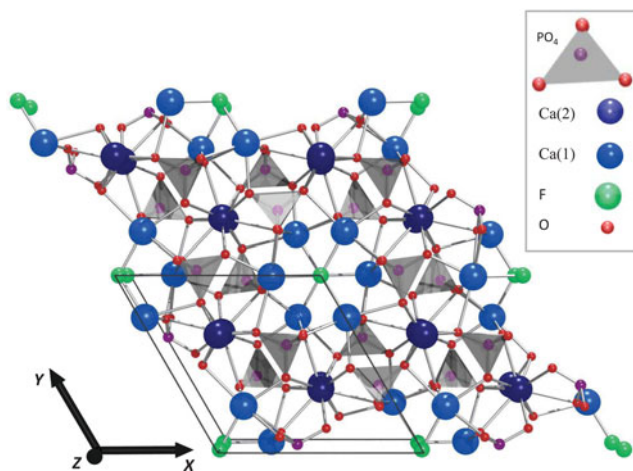Berkshire RG7 4PR, UK

Fig. 1 Schematic showing the apatite structure, with the two calcium sites indicated as dark and light blue (Ca(1) and Ca(2) sites respectively), fluorine as *green*, phosphorous ions are *purple* and oxygen ions are *red with grey* tetrahedra (Color figure online)

nudged elastic band (NEB) transition state search [9], which can determine the height and pathway of each step in the diffusion process. We investigate transport mechanisms that occur via the Ca(1) or Ca(2) sub lattices independently but also in combination. We also consider the transport of Mg^{2+}, Zn^{2+}, Sr^{2+} and Ba^{2+}, in addition to Ca^{2+}.

Methodology

Interatomic forces

The calculations presented employed a classical Born description of an ionic crystal lattice [10], based on interatomic potentials. The reactions between ion pairs are determined by two terms: (i) a long range Coulombic interaction and (ii) a short range interaction described using

parameterised pair potentials. The latter were empirically fitted to the experimentally observed properties of the material [11]. These short-range interactions act between pairs of anions, anion–cation pairs, but not pairs of cations, which are sufficiently separated (3.9 Å) that the Coulombic interaction is sufficient. The Buckingham pair potential form is used, in which two ions i and j, separated by a distance r_{ij}, interact with an energy of Φ_{ij} given by,

$$\Phi_{ij}(r_{ij}) = A_{ij}\exp\left(\frac{-r_{ij}}{\rho_{ij}}\right) - \frac{C_{ij}}{r_{ij}^6} \tag{1}$$

where A_{ij}, ρ_{ij} and C_{ij} are the empirically derived parameters [12].

The long-range Coulomb forces act between ions but not those within the same PO_4 tetrahedra. In conjunction with the Buckingham potential a Morse potential (Eq. 2) and a three body potential (Eq. 3) are used to describe the intra-ionic interactions [11] that govern the energy of the PO_4 tetrahedra, see Table 1 (detailed discussion of the potentials and their efficacy in reproducing experimental observables) has been provided previously [11, 16]).

$$\Phi_{ij}(r_{ij}) = D_{ij}(1 - e^{-\alpha(r_{ij}-r_0)})^2 - D_{ij}) \tag{2}$$

$$\Phi_{ijk}(\theta_{ijk}) = \frac{1}{2}k_{ijk}(\theta_{ijk} - \theta_0)^2 \tag{3}$$

where again D_{ij}, θ_0 and k_{ijk} are empirically determined parameters. Polarisation of oxygen anions was modelled using the shell model of Dick and Overhauser [13]; where a positively charged core is attached to a massless, negatively charged shell by a harmonic spring, as discussed by de Leeuw and Rabone [14]. These parameters have been used successfully to describe the FAp structure and to attain information on defect behaviour within the lattice [14–16]. All calculations are carried out using the GULP code [17]. The perfect lattice is simulated by defining a unit cell of ions that is repeated throughout space according to

Table 1 The Buckingham potential parameters for FAp taken from the work of Rabone and De Leeuw [11] and modified by Michie et al. [15]

Species	Parameter type	A_{ij} (eV)	ρ_{ij} (Å^{-1})	C_{ij} (eV Å^{-6})
$O_{shell}^{-1.6320} - O_{shell}^{-1.6320}$	Buckingham	16372.00	0.213	3.47
$Ca_{core}^{+2.0000} - O_{shell}^{-1.6320}$	Buckingham	1550.00	0.297	0.00
$F_{shell}^{-1.3776} - F_{shell}^{-1.3776}$	Buckingham	1317.50	0.275	13.80
$Ca_{core}^{+2.0000} - F_{shell}^{-1.3776}$	Buckingham	1550.00	0.297	0.00
$O_{shell}^{-1.6320} - F_{shell}^{-1.3776}$	Buckingham	583833.00	0.212	7.68
		D (eV)	α (Å^{-1})	r_0 (Å)
$P_{core}^{+1.1800} - O_{shell}^{-1.6320}$	Morse	3.47	2.03	1.60
		k (eV rad^{-2})	Θ_0	
$O_{shell}^{-1.6320} - P_{core}^{+1.1800} - O_{shell}^{-1.6320}$	Three body	1.323	109.47	

Each has the same core potentials for the rest of the crystal

periodic conditions. The lattice is relaxed to zero stress at constant pressure by allowing the ions and lattice parameters to vary, according to a Newton–Raphson energy minimisation procedure. The region sizes were optimised as follows; region I = 13 Å and region II = 34 Å.

Migration calculations

We begin by identifying a contiguous network of calcium sites that can facilitate bulk diffusion. Migration pathways were then determined using the nudged elastic band (NEB) technique [18]. This differs from other transition state search approaches by one key factor: the initial and final states are known and optimised to zero stress before commencing the NEB calculation. Henkelman et al. [19] concluded that the NEB method was the most efficient for transition state searches where the initial and final points are known. They compared a test example calculated with methods such as NEB, Dimer, Ridge and Drag methods, where the NEB method was the most computationally efficient and could also assess all possible saddle points and their relative heights. As such the NEB method will be utilised in this study.

The NEB approach is used to find a reaction pathway when both the initial and final states and coordinates are known. The minimum energy pathway can then be calculated between this pair of stable states; both of which are local minima on the potential energy surface. A greater discussion of this method is provided by Shepherd et al. [18].
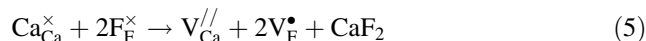
All steps taken along the NEB path are relaxed to the minimum energy through the force projection scheme, where the spring forces act along the band and potential forces act perpendicular to it, thus, the minimum energy pathway between the end points can be unambiguously identified [9, 18]. The change in the system energy (ΔE_{sys}) is then defined as the difference between the energy of the system at each step along the minimum energy pathway and the energy of the initial fully relaxed structure. The maximum value of ΔE_{sys} is the activation energy.

Cation migration in FAp can occur via a number of different mechanisms and Garcia-Fernández and González-Diaz [20] concluded a continuous network of cation migrations exists throughout the apatite lattice. In order to establish the nature of these migration pathways we will consider the migration of cations via vacancy mediated migration [21].

Work carried out by Hughes et al. [22] concluded that no interstitial sites exist that are capable of containing a calcium, as all such sites are less than 2.2 Å from an O^{2-} anion. As such, diffusion must be influenced by vacancies or structural defects, as movement via interstitial sites is not viable in $Ca_{10}(PO_4)_6F_2$ [23].

To establish the extent to which this previous conclusion might be valid, we initially calculated the calcium Frenkel energy (see Eq. 4) and compare this to the partial Schottky energy associated with removing one calcium and two fluorine ions (see Eq. 5). The (normalised) energies for these reactions are 10.4 and 5.1 eV, for the Frenkel and Schottky equations respectively. This demonstrates that the Schottky reaction is much lower in energy and thus, entirely dominant. Thus, under intrinsic defect conditions, the concentration of calcium vacancies will be orders of magnitude greater than the concentration of calcium interstitials and so vacancy migration mechanisms offer a greater flux of defects to promote calcium migration. For example at 1000 K the concentration of extrinsic calcium interstitials is calculated to be 5.2×10^{-61} while the concentration of calcium vacancies is, 6.0×10^{-10}. While this is certainly consistent with vacancy dominated migration, extrinsic doping could result in a greater concentration of interstitial calcium. However, that would require either substitution of F^- or A^+ substitution for Ca^{2+}. In the absence of these, vacancy migration will be the dominant process unless the vacancy activation energy is prohibitively high. Therefore, following the previous hypothesis [22], this study will only consider migration of cations via vacancy mechanisms.

$$Ca_{Ca}^\times \rightarrow Ca_i^{\bullet\bullet} + V_{Ca}^{//} \qquad (4)$$

$$Ca_{Ca}^\times + 2F_F^\times \rightarrow V_{Ca}^{//} + 2V_F^\bullet + CaF_2 \qquad (5)$$

In all vacancy migration pathways the movement of the vacancy is in opposition to the movement of the X^{2+} ions (where X is any of the divalent cations investigated).

Ion migrations

Cation migration

There are a number of different migration pathways for Ca^{2+} cation transport within the FAp lattice. These can be categorised into five groups; the first involves only Ca(1) sites, the second uses only Ca(2) sites and the remaining three use a combination of Ca(1) and Ca(2) sites. For each migration process a contiguous pathway across an entire unit cell has been identified and these are highlighted in Figs. 2, 3, 4, 5 and 6. In some cases migration across the cell occurs via a sequence of identical hops, but in others the pathway is via non-identical hops.

The first migration mechanism occurs via a $V_{Ca(1)}$, down the c-axis by migration between four identical sites Ca(1) → Ca(1) → Ca(1) → Ca(1) across the apatite unit cell; a plot of the migration energies as a function of reaction coordinate is presented in Fig. 2. The reaction co-ordinate is defined as the distance along the vector between the initial and final lattice points, and does not take into account any
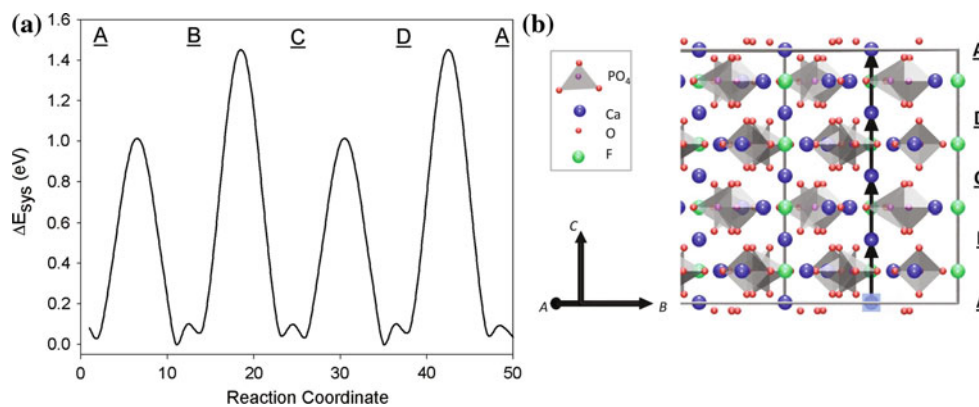
Fig. 2 Pathway 1: Graphical and schematic representations of calcium migration down the *c*-axis, via Ca(1) → Ca(1) → Ca(1) → Ca(1). **a** Activation energies for each hop. The starting point refers to the fully relaxed structure, before migration. **b** Migration pathway where *blue* atoms are calcium, *red* are oxygen, *green* are fluorine and the *grey* tetrahedra represent phosphate groups (Color figure online)

divergence from this straight line. In fact, for this particular mechanism the migration path does occur directly down the *c*-axis with no deviation in *a* and *b* directions.

The migration pathway shown in Fig. 2 describes minima only on original lattice positions for calcium atoms, that is, there are no other local minima at interstitial sites. The migration path passes through four Ca(1) sites in which two symmetrically different arrangements of surrounding PO$_4$ groups are possible. This leads to two different energy barriers for the hops a lower energy barrier of 1.0 eV and a slightly higher barrier of 1.4 eV. The activation energy for this process is therefore 1.4 eV since the highest barrier to migration is the limiting step.

The next migration mechanism considered involves only the Ca(2) sub-lattice; see Fig. 3. In the apatite structure, the Ca(2) sites form a hexagonal array about the central anion column and this migration pathway links them in a zig-zag down the *c*-axis, as shown in Fig. 3. Here the true pathway is shifted away from the backbone of the phosphate groups and inwards towards the central fluorine channel at each section of the migration. The activation energy for each of this particular series of steps is 1.1 eV.

The next three pathways all consist of a series of hops involving exchange of vacancies between Ca(1) and Ca(2) sites, in the sequence Ca(1) → Ca(2) → Ca(2) → Ca(1), across the central fluorine channel, in the basal plane. Given the number of Ca sites in the channel there are a number of possible pathways: a path that goes directly through the middle of the channel (pathways 3), one that passes at the edge of the channel (pathways 4) and one path that lies between these two (pathway 5).

Migration through the very centre of the channel (pathway 3), requires that the migrating calcium ion must pass from a Ca(1) site directly between two fluorine ions, and is illustrated in Fig. 4. Transport between two fluorine

ions gives rise to the central peak in Fig. 4 and an activation energy for migration of 5.6 eV. This migration pathway will diverge from the straightest path through the channel due to the proximity of the F$^-$ ions above and below it. However, such deviation causes it to move towards other Ca^{2+} ions which is also unfavourable, hence the exceptionally high activation energy.

Figure 5 shows pathway 4, which involves two adjacent Ca(2) sites around the periphery of the fluorine channel. Regarding the energy profile shown in Fig. 5, there are two local minima either side of the central maximum. These correspond to a split vacancy configuration. During the Ca(1)–Ca(2) migration steps the minimum energy pathway deviates towards the central fluorine channel, away from the phosphate groups. Differences in the positions of the phosphate group relative to Ca(1)–Ca(2) paths gives rise to the difference in maxima heights either side of the central minimum. The activation energy for pathway 4 is 1.7 eV.

The final migration process, pathway 5, cuts partly across the fluorine channel and is shown in Fig. 6. Again, the maximum activation energy occurs as the cation passes across the central fluorine channel; it exhibits an activation energy of 2.9 eV. Interestingly, the migration pathway deviates only slightly from a straight line, but the F$^-$ ions in the channel are displaced from their original lattice positions, away from the migrating cation.

Transport of dopant species

As a candidate nuclear waste form and for biomaterial applications, the transport of other cations in FAp is an important consideration. Therefore, the migration of Sr^{2+}, Zn^{2+}, Mg^{2+} and Ba^{2+} ions has been examined based on the same migration paths as those identified for the calcium ions.
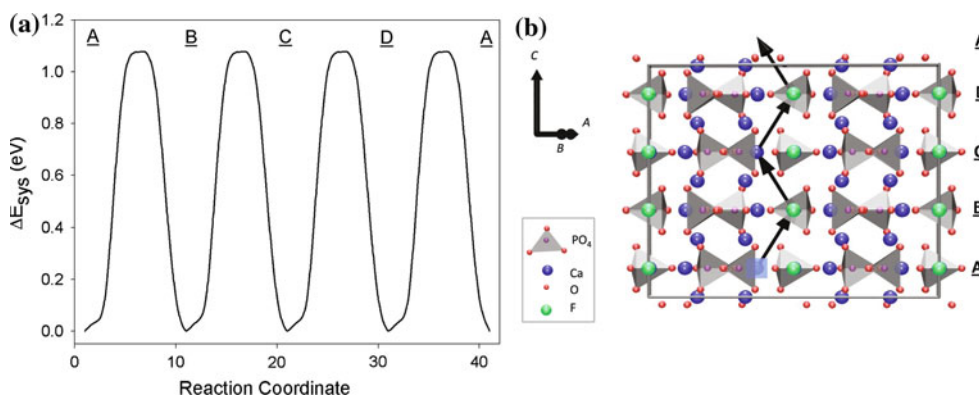
Fig. 3 Pathway 2: Graphical and schematic representations of calcium migration down the *c*-axis, via Ca(2) → Ca(2) → Ca(2) → Ca(2). **a** Activation energies for each hop. The starting point refers to the fully relaxed structure, before migration. **b** Migration pathway where *blue* atoms are calcium, *red* are oxygen, *green* are fluorine and the *grey* tetrahedra represent phosphate groups (Color figure online)
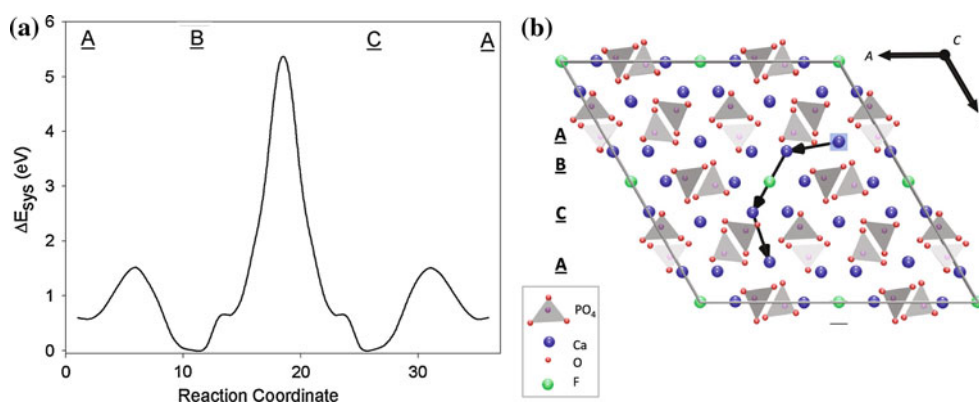

Fig. 4 Pathway 3: Graphical and schematic representations of calcium migration directly through the anion channel, via Ca(1) → Ca(2) → Ca(2) → Ca(1). **a** Activation energies for each hop. The starting point refers to the fully relaxed structure, before migration. **b** Migration pathway where *blue* atoms are calcium, *red* are oxygen, *green* are fluorine and the *grey* tetrahedra represent phosphate groups (Color figure online)
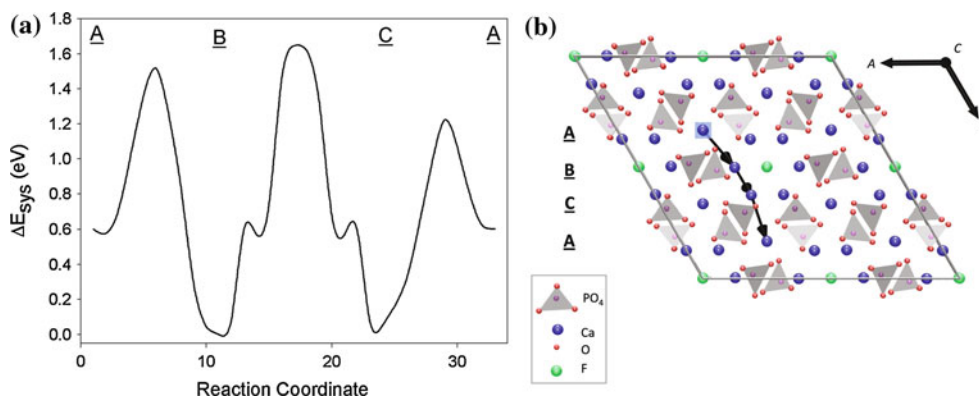

Fig. 5 Pathway 4: Graphical and schematic representations of calcium migration via the outside of the anion channel, via Ca(1) → Ca(2) → Ca(2) → Ca(1). **a** Activation energies for each hop. The starting point refers to the fully relaxed structure, before migration. **b** Migration pathway where *blue* atoms are calcium, *red* are oxygen, *green* are fluorine and the *grey* tetrahedra represent phosphate groups (Color figure online)

Each dopant cation exhibits a similar preference for migration energy pathway to those found for the Ca^{2+} ions. Results of calculated activation energies are presented in Fig. 7. Thus, as with Ca^{2+} transport, the lower energy pathway is along the *c*-axis via Ca(2) sites, though *c*-axis migration via Ca(1) sites is again only slightly higher in
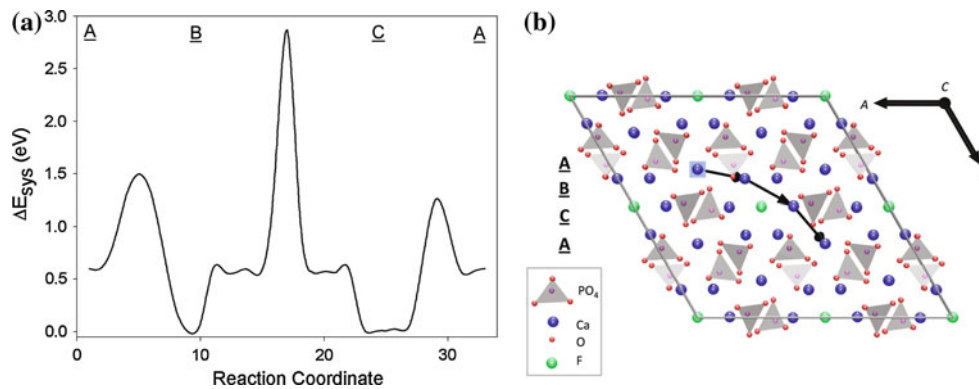
Fig. 6 Pathway 5: Graphical and schematic representations of calcium migration in-between the *c*-axis fluorine ions and the outside of the anion channel, via Ca(1) → Ca(2) → Ca(2) → Ca(1). **a** Activation energies for each hop. The starting point refers to the fully relaxed structure, before migration. **b** Migration pathway where *blue* atoms are calcium, *red* are oxygen, *green* are fluorine and the *grey* tetrahedra represent phosphate groups (Color figure online)
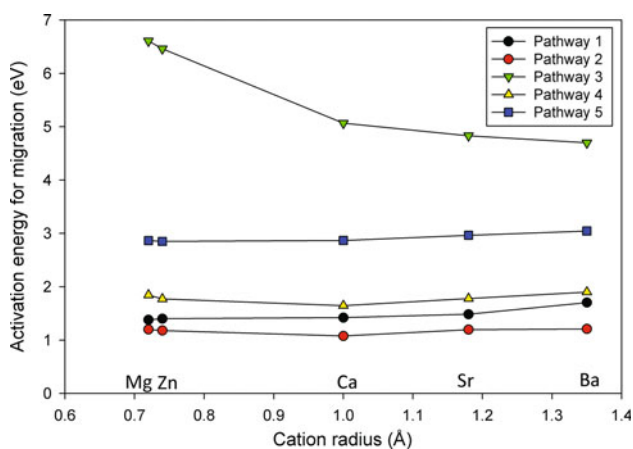

Fig. 7 Graph to show maximum activation energy of various dopant cations for the five different pathways, labeled 1–5 and described in Figs. 2, 3, 4, 5 and 6

energy in each case. Transport in the *a/b* plane is lowest in energy via pathway 4, however, this energy is sufficiently higher than those processes that operate in the *c*-axis, that it leads to distinct transport anisotropy.

If we now consider changes in activation energy as a function of cation size, overall there is at most only a very small increase in migration activation energy as atomic radius increases for pathways 1, 2, 4. Significantly, the differences in activation energy hardly change, maintaining anisotropy.

Conclusion

The results presented indicate that for Ca^{2+} transport, the lowest barriers to migration occurs for pathways 1 and 2, where the activation energies are 1.4 and 1.1 eV respectively. Both these pathways occur parallel to the *c*-axis.

There are three pathways (3–5) that can occur in the *a/b* plane, for which the lowest activation energy (pathway 4) is 1.7 eV. Therefore, considerable anisotropy in Ca^{2+} ion transport is expected with a preference for migration parallel to the *c*-axis. This preference for *c*-axis migration has previously been reported for F^- [22, 23].

The same patterns are found for other divalent cations. This suggests that divalent cation loss from FAp will occur preferentially parallel to the *c*-axis. Clearly, this will have implications for the design of any waste host based on FAp and those materials used to surround it. We note that the morphology of FAp crystallites is often reported as having a high *c/a* ratio (that is the crystallites are long and thin) [24]. This would be beneficial with regard to inhibiting the transport of divalent cations.

References

1. Hughes JM, Rakovan JF (2002) Rev Miner Geochem 48:1
2. Donald I, Metcalfe B, Fong S, Gerrard L, Strachan D, Scheele R (2007) J Nucl Mater 361:78
3. Jones F (2001) Surf Sci Rep 42:205
4. Rakovan JF, Hughes JM (2000) Can Mineral 38:839
5. Nriagu JO, Moore PB (1984) Phosphate materials. Springer-Verlag, Berlin, Heidelberg, New York, Tokyo
6. Pan YM, Fleet ME (2002) Miner Soc Am 18:13
7. Beevers B, McIntyre D (1945) Miner Mag 27:254
8. Ewing CR, Wang L (2002) Rev Miner Geochem 48:673
9. Henkelman G, Uberuaga BP, Jónsson H (2000) J Chem Phys 113:9901
10. Mayer JE (1933) J Chem Phys 1:270
11. Rabone JAL, De Leeuw NH (2006) J Comput Chem 27:253
12. Buckingham RA (1938) Proc R Soc Lond A 168:264

13. Dick BG, Overhauser AW (1958) Phys Rev 12:90
14. de Leeuw NH, Rabone JAL (2007) Cryst Eng Comm 9:1178
15. Michie EM, Grimes RW, Fong SK, Metcalfe BL (2008) J Solid State Chem 181:3287
16. EE Jay, Mallinson PM, Fong SK, Metcalfe BL, Grimes RW (2011) J Nucl Mater 414:367
17. Gale JD (1997) J Chem Soc Faraday Trans 93:629
18. Sheppard D, Rye T, Henkelman G (2008) J Chem Phys 128: 134106
19. G Henkelman, G Jóhannesson, H Jónsson (2000). In: Schwartz SD (ed) Progress on theoretical chemistry and physics. Kluwer Academic Publishers, New York, p 269
20. Garcia-Fernández P, González-Diaz PF (1980) Spectrochim Acta A 36:1069
21. Tilley RJD (2008) Defects in solids. Wiley, New York
22. Hughes JM, Cameron M, Mariano AN (1991) Am Miner 76:1165
23. Hughes JM, Cameron M, Crowley KD (1991) Am Miner 76:1857
24. Rakovan J, Reeder RJ (1996) Geochim Cosmochim Acta 60:4435